HHS Public Access

Author manuscript

Angew Chem Int Ed Engl. Author manuscript; available in PMC 2024 August 28.

Published in final edited form as:

Angew Chem Int Ed Engl. 2023 August 28; 62(35): e202305719. doi:10.1002/anie.202305719.

Supramolecular Enhancement of Electrochemical Nitrate Reduction Catalyzed by Cobalt Porphyrin Organic Cages for Ammonia Electrosynthesis in Water

Lun An[a],[b], **Mina R. Narouz**[a],[b], **Peter T. Smith**[a],[b], **Patricia De La Torre**[a],[b], **Christopher J. Chang**[a],[b],[c]

[a]Department of Chemistry, University of California, Berkeley, Berkeley, CA 94720-1460 (USA)

[b]Chemical Sciences Division, Lawrence Berkeley National Laboratory, Berkeley, CA 94720-1460 (USA)

[c]Department of Molecular and Cell Biology, University of California, Berkeley, Berkeley, CA 94720-1460 (USA)

Abstract

The electrochemical nitrate (NO_3^-) reduction reaction (NO_3RR) to ammonia (NH_3) represents a sustainable approach for denitrification to balance global nitrogen cycles and an alternative to traditional thermal Haber-Bosch processes. Here, we present a supramolecular strategy for promoting NH_3 production in water from NO_3RR by integrating two-dimensional (2D) molecular cobalt porphyrin (**CoTPP**) units into a three-dimensional (3D) porous organic cage architecture. The porphyrin box **CoPB-C8** enhances electrochemical active site exposure, facilitates substrate-catalyst interactions, and improves catalyst stability, leading to turnover numbers and frequencies for NH_3 production exceeding 200,000 and 56 s^{-1}, respectively. These values represent a 15-fold increase in NO_3RR activity and 200-mV improvement in overpotential for the 3D **CoPB-C8** box structure compared to its 2D **CoTPP** counterpart. Synthetic tuning of peripheral alkyl substituents highlights the importance of supramolecular porosity and cavity size on electrochemical NO_3RR activity. These findings establish the incorporation of 2D molecular units into 3D confined space microenvironments as an effective supramolecular design strategy for enhancing electrocatalysis.

Graphical Abstract

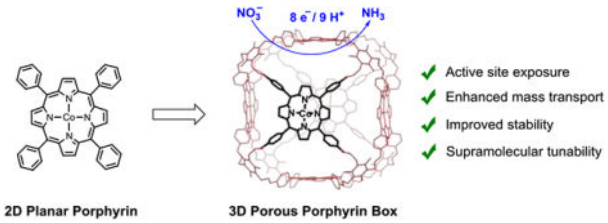

We present a supramolecular strategy for electrochemical nitrate reduction by augmenting porosity and electrochemically active sites as well as facilitating catalyst-substrate interactions. The

chrischang@berkeley.edu .

resulting 3D archtiecture enables selective ammonia production in water with greater than 90% Faradaic efficiency and turnover numbers exceeding 200,000, representing a 15-fold increase in activity and higher catalytic stability over its 2D counterpart.

Keywords

electrocatalysis; supramolecular chemistry; nitrate reduction; porous organic cage; ammonia electrosynthesis

Introduction

Denitrification, a microbially-facilitated process that reduces nitrate (NO_3^-) and nitrite (NO_2^-) to dinitrogen (N_2), plays a pivotal role in balancing the global nitrogen cycle.[1] Rising NO_3^-levels in soil and water, largely triggered by anthropogenic activities, continue to induce serious environmental and health issues by disrupting endogenous nitrogen stores.[2] Indeed, reactive nitrogen (N_r) generation has increased from ca. 30 Tg N yr^{-1} in 1968 to 226 Tg N yr^{-1} in 2020, and continues to climb.[3] Excess N_r in the environment, particularly NO_3^-, has contributed to hydrosphere deterioration,[4] ozone depletion,[5] and damage to the human endocrine system.[6] As such, developing eco-friendly processes for artificial denitrification and remediation of N_r pollution are highly needed. While physical NO_3^- removal technologies, including ion exchange,[7] reverse osmosis,[8] and electrodialysis,[9] are effective for wastewater purification, the resulting highly concentrated NO_3^-solutions require further treatment.[10]

In this context, the electrochemical nitrate reduction reaction (NO_3RR) is a potentially attractive approach to nitrogen cycle remediation as it can be powered by sustainable energy sources to form more environmentally benign and/or value-added nitrogen-based chemical products.[11] Moreover, when ammonia is the product of NO_3RR,[12] it offers an alternative route to this important industrial material and carbon-free fuel compared to the traditional thermal Haber-Bosch process. However, because the reduction of $NO_3^-$to NH_3 involves the coupled transfer of multiple electron and proton equivalents, NO_3RR selectivity is a significant challenge as various products are accessible (e.g., NO_2^-, NO, N_2O, N_2, NH_2OH).[11a] Against this background, we sought to contribute to the development of molecular electrocatalysts for NO_3RR,[13] which are far less studied relative to heterogeneous materials systems,[14] but offer untapped potential to incorporate molecular design elements to facilitate substrate-catalyst interaction and stabilize downstream reduction intermediates.

Along these lines, integrating molecular catalysts into discrete porous supramolecular architectures, such as organic cages,[15] represents an effective strategy to combine molecularly structural tailorability with material porosity and stability and offers potential to bridge the gap between homogeneous and heterogeneous catalysis; this approach has gained increasing attention in electrocatalysis design.[16] The resulting supramolecular electrocatalyst retains the intrinsic reactivities of the molecular subunits, but augments their properties by embedding them within a confined space microenvironment with size-tunable cavities. As part of a larger program in our laboratory in hybrid bioinorganic catalysis,[16b] we have leveraged individual facets of site isolation or increased surface

area for achieving electrochemical oxygen reduction reaction (ORR),[17] carbon dioxide reduction reaction (CO_2RR),[18] and hydrogen evolution reaction (HER).[19] Inspired by supramolecular systems for NO_3^-recognition[20] and transport[21] and noting that porphyrin box organic cages[22] are capable of serving as synthetic ion channels to transport nitrate anions across lipid bilayers,[23] we sought to exploit these dual features of supramolecular porosity and intrinsic NO_3^-affinity for electrochemical NO_3RR. We now report that integrating two-dimensional (2D) molecular cobalt porphyrin (**CoTPP**) catalyst units into a three-dimensional (3D) porous organic cage structure (**CoPB-C8**) markedly improves its activity and stability for electrochemical NO_3RR (Scheme 1A).[16a] This supramolecular catalyst promotes efficient NO_3RR in water with high selectivity for ammonia production (>90% Faradaic efficiency), achieving total turnover number (TON) and turnover frequency (TOF) values that exceed 200,000 (33,858 per [Co]) and 56 s^{-1} (9.4 s^{-1} per [Co]), respectively. These values represent a 15-fold improvement in NH_3 production relative to parent **CoTPP**, which can be attributed to an increase in electrochemically active cobalt centers and facilitated interactions between the supramolecular **CoPB-C8** catalyst and NO_3^- substrate. Further synthetic tuning by modifying peripheral alkyl substituents reveals the importance of cage porosity and cavity size on electrochemical NO_3RR.

Results and Discussion

Supramolecular Integration of Molecular Cobalt Porphyrin Units Increases Electroactive Metal Centers and Responses to Nitrate

To build a three-dimensional (3D) porous organic cage from two-dimensional (2D) porphyrin building blocks, the free-base porphyrin box (**PB-C8**) was first self-assembled from six tetraformylphenylporphyrin units and eight tri-amine linkers (Scheme 1B).[24] The selection of **PB-C8** was based on its potential as a synthetic ion channel to facilitate the transport of nitrate anions.[23] Metalation of the six porphyrin subunits in **PB-C8** with $CoCl_2$ yields the desired cobalt porphyrin box (**CoPB-C8**)[17a, 19] as confirmed by MALDI mass spectrometry and UV/Vis spectroscopy (Figure S25 and S26). A monomeric cobalt tetraphenylporphyrin (**CoTPP**) was used as a control compound to evaluate the effects of the supramolecular architecture. To assess electrochemical NO_3RR under aqueous conditions, both catalysts were mixed with multi-walled carbon nanotubes (MWNTs) and further deposited onto a glassy carbon electrode.[25] These working electrodes contain a catalyst loading of 5 nmol/cm^2 of **CoPB-C8** or 30 nmol/cm^2 of **CoTPP**, which normalizes the concentration of cobalt atoms in both electrodes to 30 nmol/cm^2. The CV measurements of both electrodes in 0.5 M pH 7.3 sodium sulfate (Na_2SO_4) electrolyte showed a clear Co^{III}/Co^{II} redox wave under argon (Ar),[17a, 25–26] which confirms the successful immobilization of catalysts and indicates that the intrinsic electronic properties of molecular porphyrin subunits in the supramolecular structure are not perturbed (Figure 1A and 1B). The slight positive shift of the Co^{III}/Co^{II} redox couple observed for **CoPB-C8** ($E_{1/2}$ = −0.34 V vs. saturated calomel electrode, SCE) relative to that of **CoTPP** ($E_{1/2}$ = −0.39 V vs. SCE) is likely to arise from the electron-withdrawing effect of the imine linkages in the porphyrin box. Plotting the cathodic and anodic peak currents of the Co^{III}/Co^{II} redox couple versus the scan rate gave linear correlations for both catalysts (Figure S1), enabling us to calculate the electrochemically active Co centers (EA_{Co}) for each compound using the corresponding

slope (Equation S1).[17a, 27] The calculated EA_{Co} concentration normalized per metal center was 2.16 ± 0.17 nmol/cm^2 for the **CoPB-C8** electrode and 0.44 ± 0.05 nmol/cm^2 for **CoTPP** electrode, corresponding to a 5-fold increase in electrochemically active sites upon embedding the 2D Co porphyrin unit within a 3D porous supramolecular structure (7.2% electroactive Co in **CoPB-C8** vs. 1.4% in **CoTPP**). Upon titration with sodium nitrate ($NaNO_3$) (Figure S2A and S2B), a much larger catalytic current was observed for **CoPB-C8** over **CoTPP** electrode (Figure 1C), indicating superior NO_3RR activity for **CoPB-C8**. As a control experiment, the catalyst-free glassy carbon electrode shows negligible NO_3RR activity, confirming that the catalytic currents indeed arise from the cobalt compounds (Figure S2C).

We hypothesized that compared to gaseous CO_2 and O_2 substrates, studies of potential substrate-catalyst interactions within supramolecular electrocatalyst systems would be more feasible with solution NO_3^-via spectroscopic techniques such as nuclear magnetic resonance (NMR) spectroscopy. Indeed, we were able to observe direct interactions between the supramolecular catalyst platform and NO_3^-substrate by ^{1}H-NMR spectroscopy titration experiments (Figure S3). The addition of tetrabutylammonium nitrate ($TBANO_3$) to a diamagnetic and soluble zinc porphyrin box[28] congener (Figure 1D) in CD_3CN solvent led to apparent upfield shifts of protons on the porphyrinic phenyl rings, whereas no shift was observed for the imine protons (a) or the pyrrolic protons (b) (Figure 1E). Interestingly, only the protons at the ortho-position (c) of the imine substituent shifted while the chemical shift of protons at the meta-position (d) remained unchanged, which indicates a possible anion-**π** interaction of the negative charged $NO_3^-$and partially positive charged porphyrinic phenyl rings induced by the adjacent electron-withdrawing imine group.[29] We reasoned that the interaction between the supramolecular cage and NO_3^-substrate could potentially facilitate mass transport and thus enhance catalytic performance.[23]

Supramolecular Cobalt Porphyrin Box Catalyst Shows Enhanced Reactivity and Stability Over Parent Porphyrin for Electrochemical NO_3RR With Ammonia as the Major Product

We next performed controlled potential electrolysis (CPE) experiments with product detection in 0.5 M Na_2SO_4 with added 0.1 M $NaNO_3$ under an Ar atmosphere. Under these conditions, both **CoPB-C8** and **CoTPP** selectively produced NH_3 with Faradaic efficiencies (FE) reaching greater than 90% over a range of applied potentials (−1.04 to −1.54 V vs. SCE) (Figure 2A). Importantly, **CoPB-C8** showed superior reactivity for NH_3 production, which starts to generate NH_3 at an onset potential of −0.94 V vs. SCE with an NH_3 yield rate of 16.7 μg h^{-1} (Figure 2B), while **CoTPP** required a 200 mV more negative applied potential (-1.14 V vs. SCE) to achieve a similar NH_3 production rate (14.2 μg h^{-1}). These results are in line with the CV data (Figure 1C) and establish a supramolecular enhancement for electrochemical NO_3RR. Along the applied potentials, **CoPB-C8** showed superior NH_3 partial current density than **CoTPP** (Figure S6), of which the largest difference in catalytic activity for the two compounds was observed at −1.14 V vs. SCE with a 15-fold increase in NH_3 yield rate for the **CoPB-C8** electrode (221.5 μg h^{-1}) over the **CoTPP** electrode (14.2 μg h^{-1}), thus demonstrating the advantages of integrating a molecular electrocatalyst into a supramolecular matrix. After electrolysis at −1.54 V vs. SCE for 1 h, **CoPB-C8** produced 2,729 μg of NH_3 with a turnover number (TON) per cobalt center of 5,343 (Figure 2D).

Further optimization of catalyst loading showed that the concentration of **CoPB-C8** can be lowered to 0.5 nmol/cm^2 while still maintaining good electrochemical NO_3RR activity, resulting in TON values reaching 208,998 (TON = 34,833 per Co) after 1 h, corresponding to a turnover frequency (TOF) of 56 s^{-1} (TOF = 9.4 s^{-1} per Co) (Figure 2E), rendering **CoPB-C8** a highly efficient electrochemical NO_3RR catalyst under aqueous conditions (Table S2).

Moreover, embedding the molecular cobalt porphyrin unit into a supramolecular porous cage increases catalyst stability. Stable NH_3 production was observed for **CoPB-C8** over longer-term CPEs at −1.34 V vs. SCE (Figure 2C), where this catalyst kept producing NH_3 at a relatively constant rate of 1,358 μg/h to produce a total of 5,432 μg of NH_3 during the 4-h electrolysis, while maintaining a high FE of 95%. In contrast, **CoTPP** loses significant activity after 1.5 h with the NH_3 yield nearing a plateau, resulting in only 825 μg of NH_3 being produced after 4 h with a lower FE of 78% (Figures S7 and S8). We speculate that this improved stability likely arises from the isolated cobalt site in the PB architecture, which can prevent catalyst deactivation pathways.[17a, 30] Next, we used ^{1}H-NMR to validate the generation of NH_3 by electrochemical NO_3RR catalysis, including with ^{15}N-labeled substrate. Indeed, a set of three symmetric peaks with a spacing of 51 Hz corresponding to $^{14}NH_4^+$ were observed after electrolysis at −1.44 V vs. SCE in $NaNO_3$ electrolyte (Figure 2F). Moreover, a doublet peak ($J_{N\text{-}H}$ = 72 Hz) attributed to $^{15}NH_4^+$ was detected when using isotopic ^{15}N labeled $Na^{15}NO_3$ electrolyte (Figure 2F), thus confirming that $NO_3^-$is indeed the nitrogen source for the observed NH_3 product.

Nitrite and Hydroxylamine Are Competent Intermediates in Ammonia Electrosynthesis Catalyzed by the Supramolecular Cobalt Porphyrin Box

Nitrite (NO_2^-), the two-electron reduction product of NO_3^-, is another major water pollutant that is even more potentially harmful than NO_3^-.[11d] Thus, efficient catalysts for the electrochemical NO_2^-reduction reaction (NO_2RR) are desired for developing effective denitrification and chemical production. While several types of molecular catalysts have shown activity towards electrochemical NO_2RR, achieving NH_3 selectivity with a sufficiently high rate of product generation remains challenging.[31] Recently, a graphite conjugated diimine macrocyclic cobalt catalyst has been reported to reduce NO_2^-selectively to NH_3 with TOF up to 14.4 s^{-1} when using a glassy carbon electrode.[32] We performed electrochemical NO_2RR with the **CoPB-C8** catalyst to compare its reactivity with reported systems and determine whether NO_2^-could be a competent intermediate during our electrochemical NO_3RR system. Electrochemical NO_2RR was assayed in a similar manner to electrochemical NO_3RR except for the use of $NaNO_2$ as a substrate (0.1 M). As shown in Figure 3A, a greater catalytic current was observed for the **CoPB-C8** electrode compared to the **CoTPP** electrode by CV (Figure S9), indicating higher electrochemical NO_2RR for the former catalyst. Indeed, CPE experiments revealed that **CoPB-C8** showed superior activity to **CoTPP** for NO_2RR (Figures 3B and S10), with NH_3 detected as the major product (Figure S11). Under optimized conditions, the highest NO_2RR TON of 238932 (39822 per Co center) was obtained with 0.5 nmol/cm^2 **CoPB-C8** loading at −1.44 vs. SCE after 1 h, corresponding to a TOF of 66.6 s^{-1} (11.1 s^{-1} per [Co]) (Figure S12). These data establish that **CoPB-C8** is an efficient catalyst for electrochemical NO_2^-reduction, comparable to

the high-performing NO_2RR systems reported in the literature.[33] The magnitude of the observed activity enhancement for **CoPB-C8** over **CoTPP** is smaller for NO_2RR than for NO_3RR. For example, at the applied potential of −1.14 V vs. SCE, **CoPB-C8** exhibited a ca. 2.6-fold increase in NH_3 yield rate over **CoTPP** for NO_2RR, relative to the 15-fold enhancement for NO_3RR, thus demonstrating that the porous supramolecular structure of **CoPB-C8** more strongly facilitates the rate-determining step of nitrate to nitrite reduction in the electrochemical NO_3RR.

Finally, hydroxylamine (NH_2OH) has been proposed as another key intermediate in both electrochemical NO_3RR and NO_2RR but often requires the use of a special metal electrode, such as Hg or Cu, to ultimately form NH_3.[11c] For our **CoPB-C8** electrode, a CPE experiment in 0.5 M Na_2SO_4/0.1 M NH_2OH electrolyte with potential holding at −1.34 V vs. SCE exhibited >99% FE for NH_3 production, confirming that NH_2OH can also behave as a substrate for electrocatalytic NH_3 generation in our platform (Figure S13). The collective results show that the supramolecular porphyrin box catalyst platform is capable of sequential electrochemical reductions to convert NO_3^- to NH_3, but under catalytic conditions does not release partially reduced NO_2^- or NH_2OH intermediates. These findings highlight the ability of this supramolecular architecture to funnel intermediates to desirable product pathways.

Synthetic Tuning of Peripheral Alkyl Substituents on the Supramolecular Box Structure Highlight the Importance of Box Porosity and Cavity Size on Ammonia Electrosynthesis by NO_3RR

With these results in hand, we sought to further optimize the catalytic performance of this supramolecular electrocatalyst platform for NO_3RR by tuning peripheral structure. We have achieved gains in CO_2RR by appending remote positive charges into supramolecular scaffolds.[28] In this instance, we hypothesized that tuning the lengths of peripheral alkyl chains on these **CoPB** catalysts with a conserved supramolecular core would show measurable effects on electrochemical NO_3RR activity and provide direct structure-activity relationships to assess contributions of supramolecular porosity. To this end, we synthesized **CoPB-C4** bearing shorter butyl ($-C_4H_9$) substituents and **CoPB-C13'** bearing longer 6-(hexyloxy)hexyl ($-(CH_2)_6OC_6H_{13}$) substituents relative to the octyl ($-C_8H_{17}$) groups in **CoPB-C8**. The electrochemical NO_3RR activities of these **CoPBs** are summarized in Figure 4. While **CoPB-C4** showed a similar supramolecular enhancement for NH_3 production, the porous cage effect on electrochemical NO_3RR of **CoPB-13'** was totally suppressed, resulting in a similar reactivity to the nonporous **CoTPP**. We suggest that the loss of the supramolecular enhancement for NO_3RR in **CoPB-13'** is likely due to substantial blocking of the cage windows and access to the porous cavity by the longer alkyl chains, with subsequent suppression of nitrate binding and transport. To further assess the effects of alkyl substituent lengths on box porosity and cavity size, we performed molecular dynamics (MD) simulations to obtain the lowest energy conformers of these **CoPBs** (Figure S14).[17a, 34] We then used a python package, named pywindow,[35] to calculate the average window diameter (D_{window}) and intrinsic void diameter (D_{void}) of this family of **CoPBs** (Table S1). As expected, the inclusion of longer alkyl chains in the **CoPB** structures results in decreased D_{window} values as listed in Table S1. While **CoPB-C8** (4.2 Å) still retains comparable D_{window} to **CoPB-C4** (6.0 Å), the D_{window} of **CoPB-C13'** decreased

to 2.1 Å, which is much smaller than the hydrodynamic radius of nitrate (3.16 Å),[36] thus suppressing NO_3RR for this catalyst. It is noteworthy that the calculated D_{window} for **CoPB-C4** (6.0 Å) is close to the window size obtained from the crystal structure of the metal free **PB-C4** (6.6 × 8.5 Å),[24] thus demonstrating the reliability of current calculation and indicating negligible structure change of PBs after metalation. The observed correlation between NO_3RR reactivity and the cage window size indicates that, despite the presence of multiple potential catalytic sites and significant differences in molecular weight, these CoPBs can be considered as single molecular catalyst entities. Importantly, this correlation suggests that it is feasible to manipulate and adjust the reactivity of these catalysts through synthetic chemistry. Interestingly, the calculated D_{void} values for **CoPB-C4** (18.92 Å) and **CoPB-C8** (18.71 Å) remained constant, indicating that even the octyl substituent is not long enough to occupy the space inside the cage. However, the calculated D_{void} value decreased significantly for **CoPB-C13'** (11.85 Å), presumably due to its much longer alkyl substituents. Taken together, these findings reveal the importance of box porosity and cavity size on electrochemical NO_3RR, which will be helpful in establishing design rules for broader exploration of supramolecular electrocatalysis.

Conclusion

To close, we have presented a supramolecular strategy to enhance electrochemical NO_3RR catalysis through integrating a monomeric two-dimensional (2D) cobalt porphyrin electrocatalyst into a three-dimensional (3D) porphyrin-based porous organic cage architecture. The resulting supramolecular electrocatalyst, **CoPB-C8**, is capable of increasing active site exposure and electrochemically active sites, as well as facilitating catalyst-substrate interactions. These combined features enable selective NO_3RR to NH_3 product in water with greater than 90% Faradaic efficiency and turnover numbers exceeding 200,000, representing a 15-fold increase in activity, a 200-mV improvement in overpotential, and higher catalytic stability for ammonia electrosynthesis catalyzed by the 3D structure over its 2D counterpart. Moreover, this 3D box platform is competent for selective nitrate-to-ammonia conversion via sequential multi-electron reduction processes, without releasing nitrite or hydroxylamine intermediates. Finally, synthetic tuning of peripheral alkyl substituents reveal the importance of box porosity and cavity size on electrochemical NO_3RR activity. This work provides a starting point for using bioinspired, supramolecular design principles for developing catalysts for electrochemical reduction processes related to the nitrogen cycle and a broader range of small-molecule substrates, particularly oxyanions that are important in water remediation and energy storage.

Supplementary Material

Refer to Web version on PubMed Central for supplementary material.

Acknowledgements

This work was supported by the U.S. Department of Energy, Office of Science, Office of Advanced Scientific Computing, Office of Basic Energy Sciences, via the Division of Chemical Sciences, Geosciences, and Bioscience of the U.S. Department of Energy at Lawrence Berkeley National Laboratory (Grant No. DE-AC02-05CH11231 to C.J.C.). C.J.C. is a CIFAR Fellow. L.A. thanks SIOC/Pharmaron for a postdoctoral fellowship. M.R.N. acknowledges NSERC (Canada) for a postdoctoral fellowship. P.T.S. and P.D.T. acknowledge the NSF for Graduate

Research Fellowships. We thank Dr. Hasan Celik in the UC Berkeley College of Chemistry NMR facility (CoC-NMR) for technical assistance and Prof. Kimoon Kim (POSTECH) for helpful discussions. Instruments in the CoC-NMR are supported in part by NIH (S10OD024998). We also thank the College of Chemistry's Molecular Graphics and Computation Facility, which is supported by the NIH (S10OD023532), for computational resources.

References

[1]. Kuypers MMM, Marchant HK, Kartal B, Nat. Rev. Microbiol 2018, 16, 263–276. [PubMed: 29398704]

[2]. Zhang X, Ward BB, Sigman DM, Chem. Rev 2020, 120, 5308–5351. [PubMed: 32530264]

[3]. a)Galloway JN, Bleeker A, Erisman JW, Annu. Rev. Environ. Resour 2021, 46, 255–288;b)Galloway JN, Townsend AR, Erisman JW, Bekunda M, Cai Z, Freney JR, Martinelli LA, Seitzinger SP, Sutton MA, Science 2008, 320, 889–892. [PubMed: 18487183]

[4]. Bijay S, Craswell E, SN Appl. Sci 2021, 3, 518.

[5]. Lehnert N, Dong HT, Harland JB, Hunt AP, White CJ, Nat. Rev. Chem 2018, 2, 278–289.

[6]. Ward MH, Jones RR, Brender JD, De Kok TM, Weyer PJ, Nolan BT, Villanueva CM, Van Breda SG, Int. J. Env. Res. Public Health 2018, 15, 1557. [PubMed: 30041450]

[7]. Werth CJ, Yan CX, Troutman JP, Acs Es&T Engineering 2021, 1, 6–20.

[8]. Scholes RC, Vega MA, Sharp JO, Sedlak DL, Environ. Sci.: Water Res. Technol 2021, 7, 650–661.

[9]. Rivera FF, Rivero EP, Castaneda-Zaldivar F, Ind. Eng. Chem. Res 2021, 60, 5014–5023.

[10]. Barrabés N, Sá J, Appl. Catal., B 2011, 104, 1–5.

[11]. a)Rosca V, Duca M, de Groot MT, Koper MTM, Chem. Rev 2009, 109, 2209–2244; [PubMed: 19438198] b)Duca M, Koper MTM, Energy Environ. Sci 2012, 5, 9726–9742;c)Zeng Y, Priest C, Wang G, Wu G, Small Methods 2020, 4, 2000672;d)Min B, Gao Q, Yan Z, Han X, Hosmer K, Campbell A, Zhu H, Ind. Eng. Chem. Res 2021, 60, 14635–14650.

[12]. a)van Langevelde PH, Katsounaros I, Koper MTM, Joule 2021, 5, 290–294;b)Qing G, Ghazfar R, Jackowski ST, Habibzadeh F, Ashtiani MM, Chen C-P, Smith MR, Hamann TW, Chem. Rev 2020, 120, 5437–5516; [PubMed: 32459470] c)Valera-Medina A, Amer-Hatem F, Azad AK, Dedoussi IC, de Joannon M, Fernandes RX, Glarborg P, Hashemi H, He X, Mashruk S, McGowan J, Mounaim-Rouselle C, Ortiz-Prado A, Ortiz-Valera A, Rossetti I, Shu B, Yehia M, Xiao H, Costa M, Energy Fuels 2021, 35, 6964–7029;d)Hao D, Liu Y, Gao S, Arandiyan H, Bai X, Kong Q, Wei W, Shen PK, Ni B-J, Mater. Today 2021, 46, 212–233.

[13]. a)Taniguchi I, Nakashima N, Matsushita K, Yasukouchi K, J. Electroanal. Chem 1987, 224, 199–209;b)Chebotareva N, Nyokong T, J. Appl. Electrochem 1997, 27, 975–981;c)Shen J, Birdja YY, Koper MTM, Langmuir 2015, 31, 8495–8501; [PubMed: 26154347] d)Xu S, Ashley DC, Kwon HY, Ware GR, Chen CH, Losovyj Y, Gao XF, Jakubikova E, Smith JM, Chem. Sci 2018, 9, 4950–4958; [PubMed: 29938022] e)Braley SE, Ashley DC, Jakubikova E, Smith JM, Chem. Commun 2020, 56, 603–606;f)Partovi S, Xiong ZQ, Kulesa KM, Smith JM, Inorg. Chem 2022, 61, 9034–9039. [PubMed: 35666148]

[14]. a)Li J, Zhan GM, Yang JH, Quan FJ, Mao CL, Liu Y, Wang B, Lei FC, Li LJ, Chan AWM, Xu LP, Shi YB, Du Y, Hao WC, Wong PK, Wang JF, Dou SX, Zhang LZ, Yu JC, J. Am. Chem. Soc 2020, 142, 7036–7046; [PubMed: 32223152] b)Chen GF, Yuan YF, Jiang HF, Ren SY, Ding LX, Ma L, Wu TP, Lu J, Wang HH, Nat. Energy 2020, 5, 605–613;c)Wu ZY, Karamad M, Yong X, Huang Q, Cullen DA, Zhu P, Xia C, Xiao Q, Shakouri M, Chen FY, Kim JYT, Xia Y, Heck K, Hu Y, Wong MS, Li Q, Gates I, Siahrostami S, Wang H, Nat Commun 2021, 12, 2870; [PubMed: 34001869] d)Gao Z, Lai YL, Tao Y, Xiao LH, Zhang LX, Luo F, ACS Cent. Sci 2021, 7, 1066–1072; [PubMed: 34235267] e)Gao Q, Yao B, Pillai HS, Zang W, Han X, Liu Y, Yu S-W, Yan Z, Min B, Zhang S, Zhou H, Ma L, Xin H, He Q, Zhu H, Nat. Synth 2023, 10.1038/s44160-023-00258-x;f)Lv Y, Ke SW, Gu YM, Tian BL, Tang LY, Ran P, Zhao Y, Ma J, Zuo JL, Ding MN, Angew. Chem. Int. Ed 2023, 10.1002/anie.202305246.

[15]. a)Tozawa T, Jones JTA, Swamy SI, Jiang S, Adams DJ, Shakespeare S, Clowes R, Bradshaw D, Hasell T, Chong SY, Tang C, Thompson S, Parker J, Trewin A, Bacsa J, Slawin AMZ, Steiner A, Cooper AI, Nature Mater 2009, 8, 973–978; [PubMed: 19855385] b)Diercks CS, Yaghi OM, Science 2017, 355, eaal1585. [PubMed: 28254887]

[16]. a)Banerjee S, Anayah RI, Gerke CS, Thoi VS, ACS Cent. Sci 2020, 6, 1671–1684; [PubMed: 33145407] b)Smith PT, Nichols EM, Cao Z, Chang CJ, Acc. Chem. Res 2020, 53, 575–587; [PubMed: 32124601] c)Proppe AH, Li YGC, Aspuru-Guzik A, Berlinguette CP, Chang CJ, Cogdell R, Doyle AG, Flick J, Gabor NM, van Grondelle R, Hammes-Schiffer S, Jaffer SA, Kelley SO, Leclerc M, Leo K, Mallouk TE, Narang P, Schlau-Cohen GS, Scholes GD, Vojvodic A, Yam VWW, Yang JY, Sargent EH, Nat. Rev. Mater 2020, 5, 828–846.

[17]. a)Smith PT, Kim Y, Benke BP, Kim K, Chang CJ, Angew. Chem. Int. Ed 2020, 59, 4902–4907;b)Oldacre AN, Friedman AE, Cook TR, J. Am. Chem. Soc 2017, 139, 1424–1427. [PubMed: 28102678]

[18]. a)Smith PT, Benke BP, Cao Z, Kim Y, Nichols EM, Kim K, Chang CJ, Angew. Chem. Int. Ed 2018, 57, 9684–9688;b)Hu Y, Huang S, Wayment LJ, Wu J, Xu Q, Chang T, Chen Y-P, Li X, Andi B, Chen H, Jin Y, Zhu H, Du M, Lu S, Zhang W, Cell Rep. Phys. Sci 2023, 4, 101285.

[19]. Smith PT, Benke BP, An L, Kim Y, Kim K, Chang CJ, ChemElectroChem 2021, 8, 1653–1657.

[20]. a)Barendt TA, Docker A, Marques I, Felix V, Beer PD, Angew. Chem. Int. Ed 2016, 55, 11069–11076;b)Lauer JC, Bhat AS, Barwig C, Fritz N, Kirschbaum T, Rominger F, Mastalerz M, Chem.Eur.J 2022, 28, e202201527; [PubMed: 35699158] c)Langton MJ, Beer PD, Chem. Commun 2014, 50, 8124–8127.

[21]. Wu X, Howe ENW, Gale PA, Acc. Chem. Res 2018, 51, 1870–1879. [PubMed: 30063324]

[22]. Mukhopadhyay RD, Kim Y, Koo J, Kim K, Acc. Chem. Res 2018, 51, 2730–2738. [PubMed: 30345738]

[23]. Benke BP, Aich P, Kim Y, Kim KL, Rohman MR, Hong S, Hwang IC, Lee EH, Roh JH, Kim K, J. Am. Chem. Soc 2017, 139, 7432–7435. [PubMed: 28538099]

[24]. Hong S, Rohman MR, Jia J, Kim Y, Moon D, Kim Y, Ko YH, Lee E, Kim K, Angew. Chem. Int. Ed 2015, 54, 13241–13244.

[25]. Hu XM, Ronne MH, Pedersen SU, Skrydstrup T, Daasbjerg K, Angew. Chem. Int. Ed 2017, 56, 6468–6472.

[26]. Cheng SH, Su YO, Inorg. Chem 1994, 33, 5847–5854.

[27]. Wang M, Torbensen K, Salvatore D, Ren S, Joulié D, Dumoulin F, Mendoza D, Lassalle-Kaiser B, Işci U, Berlinguette CP, Robert M, Nat. Commun 2019, 10, 3602. [PubMed: 31399585]

[28]. An L, De La Torre P, Smith PT, Narouz MR, Chang CJ, Angew. Chem. Int. Ed 2023, 62, e202209396.

[29]. a)Adriaenssens L, Estarellas C, Jentzsch AV, Belmonte MM, Matile S, Ballester P, J. Am. Chem. Soc 2013, 135, 8324–8330; [PubMed: 23672588] b)Wang DX, Wang MX, Acc. Chem. Res 2020, 53, 1364–1380; [PubMed: 32559061] c)Watt MM, Zakharov LN, Haley MM, Johnson DW, Angew. Chem. Int. Ed 2013, 52, 10275–10280.

[30]. Ali A, Akram W, Liu H-Y, Molecules 2019, 24, 78.

[31]. a)Xu S, Kwon HY, Ashley DC, Chen CH, Jakubikova E, Smith JM, Inorg. Chem 2019, 58, 9443–9451; [PubMed: 31251052] b)Guo YX, Stroka JR, Kandemir B, Dickerson CE, Bren KL, J. Am. Chem. Soc 2018, 140, 16888–16892; [PubMed: 30457856] c)Stroka JR, Kandemir B, Matson EM, Bren KL, ACS Catal. 2020, 10, 13968–13972.

[32]. Braley SE, Xie JZ, Losovyj Y, Smith JM, J. Am. Chem. Soc 2021, 143, 7203–7208. [PubMed: 33939918]

[33]. Zhang X, Wang YT, Wang YB, Guo YM, Xie XY, Yu YF, Zhang B, Chem. Commun 2022, 58, 2777–2787.

[34]. Berardo E, Greenaway RL, Turcani L, Alston BM, Bennison MJ, Miklitz M, Clowes R, Briggs ME, Cooper AI, Jelfs KE, Nanoscale 2018, 10, 22381–22388. [PubMed: 30474677]

[35]. Miklitz M, Jelfs KE, J. Chem. Inf. Model 2018, 58, 2387–2391. [PubMed: 30199639]

[36]. Marcus Y, Chem. Rev 1988, 88, 1475–1498.

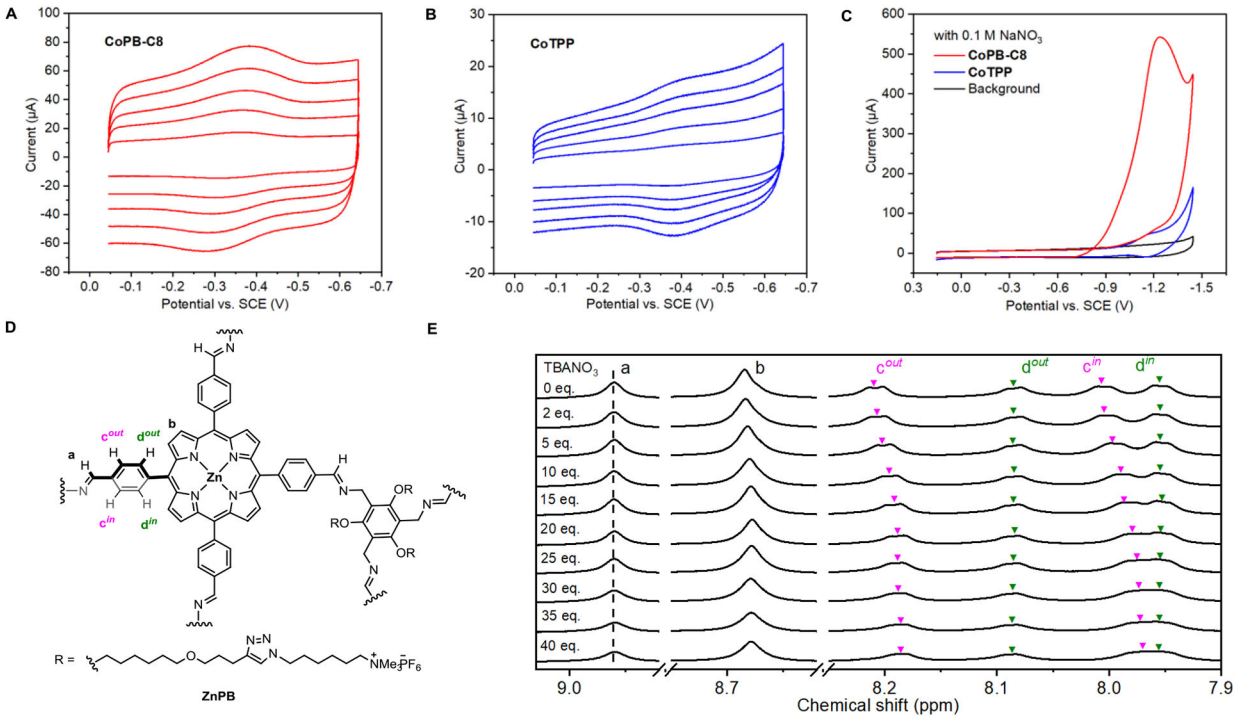

Figure 1.

The supramolecular cobalt porphyrin box organic cage **CoPB-C8** shows an increase in electroactive metal sites and superior electrochemical nitrite reduction reaction (NO_3RR) activity relative to the parent cobalt tetraphenylporphyrin (**CoTPP**) control analog. Scan rate dependence from 0.1 to 0.5 V/s of the Co^{III}/Co^{II} redox couples for (A) supramolecular **CoPB-C8** and (B) molecular **CoTPP** catalyst electrodes in 0.5 M pH 7.3 aqueous Na_2SO_4 solution under an Ar atmosphere. Each catalyst electrode was prepared by depositing 30 nmol/cm^2 Co (5.0 nmol/cm^2 of **CoPB-C8** and 30.0 nmol/cm^2 of **CoTPP**). Plotting the corresponding cathodic and anodic peak currents against the scan rate indicated 1.4% of Co centers are electroactive in the **CoTPP** film and 7.2% of the Co centers are electroactive in the **CoPB-C8** film. (C) CV traces for **CoPB-C8** (red), **CoTPP** (blue), and electrode background (black) obtained in 0.5 M Na_2SO_4/0.1 M $NaNO_3$ saturated with Ar. (D) Chemical structure of the zinc porphyrin cage (**ZnPB**) modified for solubility used for ^{1}H-NMR titration experiments. (E) ^{1}H NMR titration of a diamagnetic analog of the supramolecular porphyrin catalyst, **ZnPB** (1 eq.), with varying concentrations of tetrabutylammonium nitrate ($TBANO_3$) (0–40 eq.), revealing a host-guest interaction between the porphyrin box host and nitrate anion guest.

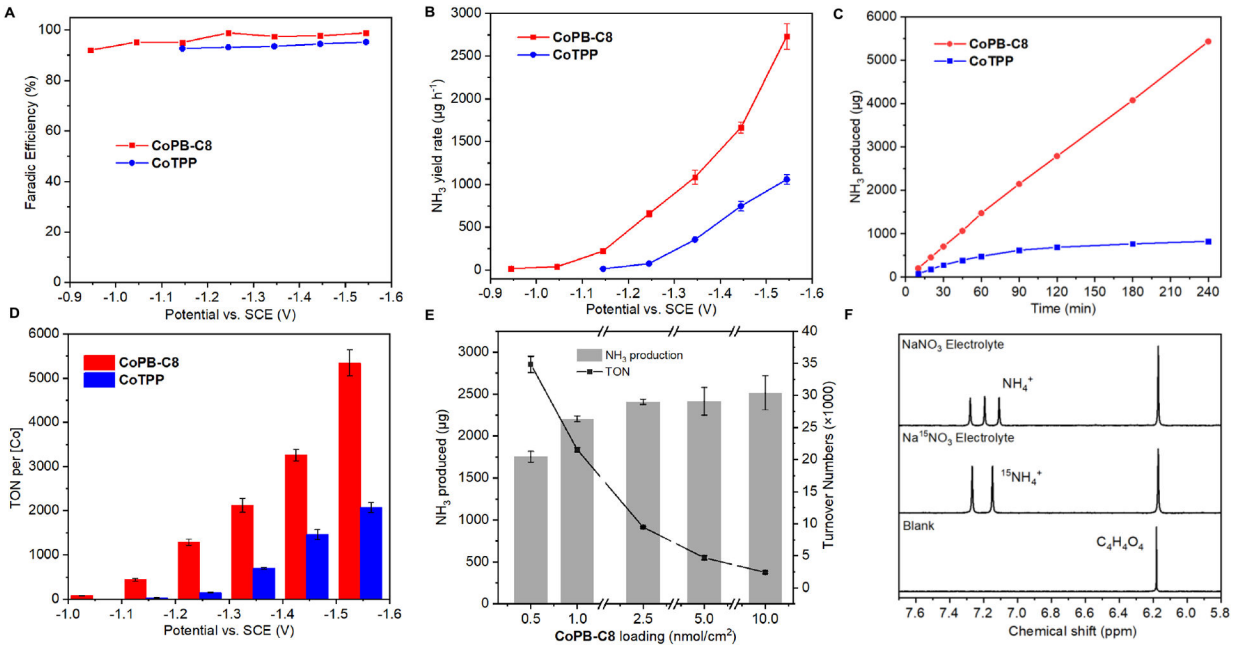

Figure 2.

Supramolecular cobalt porphyrin box organic cage shows superior electrochemical nitrate reduction (NO_3RR) activity relative to a parent cobalt tetraphenylporphyrin control analog. (A) Faradaic efficiency (FE) for electrochemical nitrate reduction to ammonia, plotted by NH_3 production, catalyzed by **CoPB-C8** (red) and **CoTPP** (blue) over a range of applied potentials after 1 h electrolysis. (B) NH_3 yield rate for **CoPB-C8** (red), and **CoTPP** (blue). (C) NH_3 production during 4 h electrolysis at −1.34 V vs. SCE for **CoPB-C8** (red), and **CoTPP** (blue). (D) Comparison of turnover number (TON) values per Co over a range of applied potentials after 1 h electrolysis. (E) NH_3 production and TON for various amounts of **CoPB-C8** loading at −1.54 V vs. SCE. (F) ^1H NMR spectra showing direct detection of NH_3 product with ^{15}N labeling of substrate for electrolysis runs, after three independent nitrate reduction tests at −1.44 V vs SCE, 0.5 M Na_2SO_4/0.1 M $NaNO_3$, 0.5 M Na_2SO_4/0.1 M $Na^{15}NO_3$, and 0.5 M Na_2SO_4. Maleic acid ($C_4H_4O_4$) was added as an internal standard.

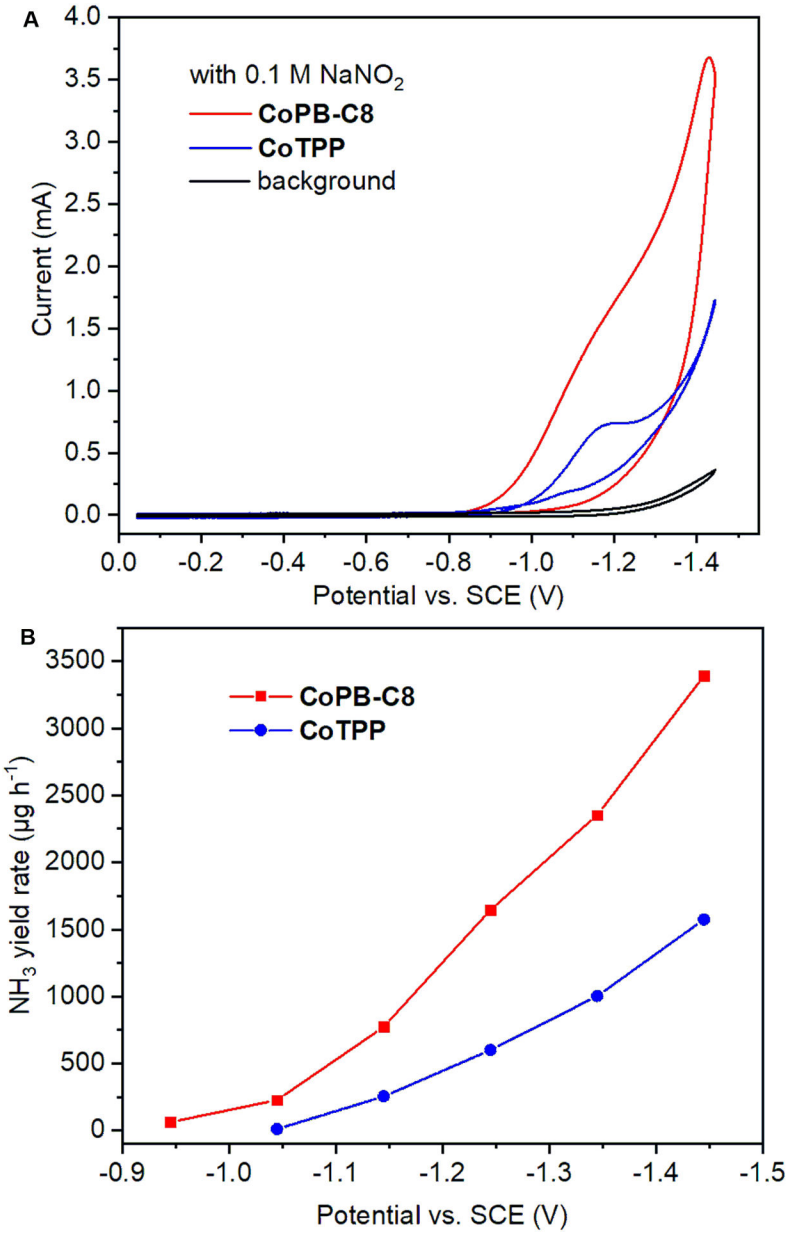

Figure 3.

Supramolecular cobalt porphyin box organic cage shows superior electrochemical nitrite reduction activity relative to a cobalt tetraphenylporphyrin control analog. (A) CV traces for **CoPB-C8** (red), **CoTPP** (blue), and electrode background (black) obtained in 0.5 M Na_2SO_4/0.1 M $NaNO_2$ saturated with Ar. (B) NH_3 yield rate for **CoPB-C8** (red), and **CoTPP** (blue).

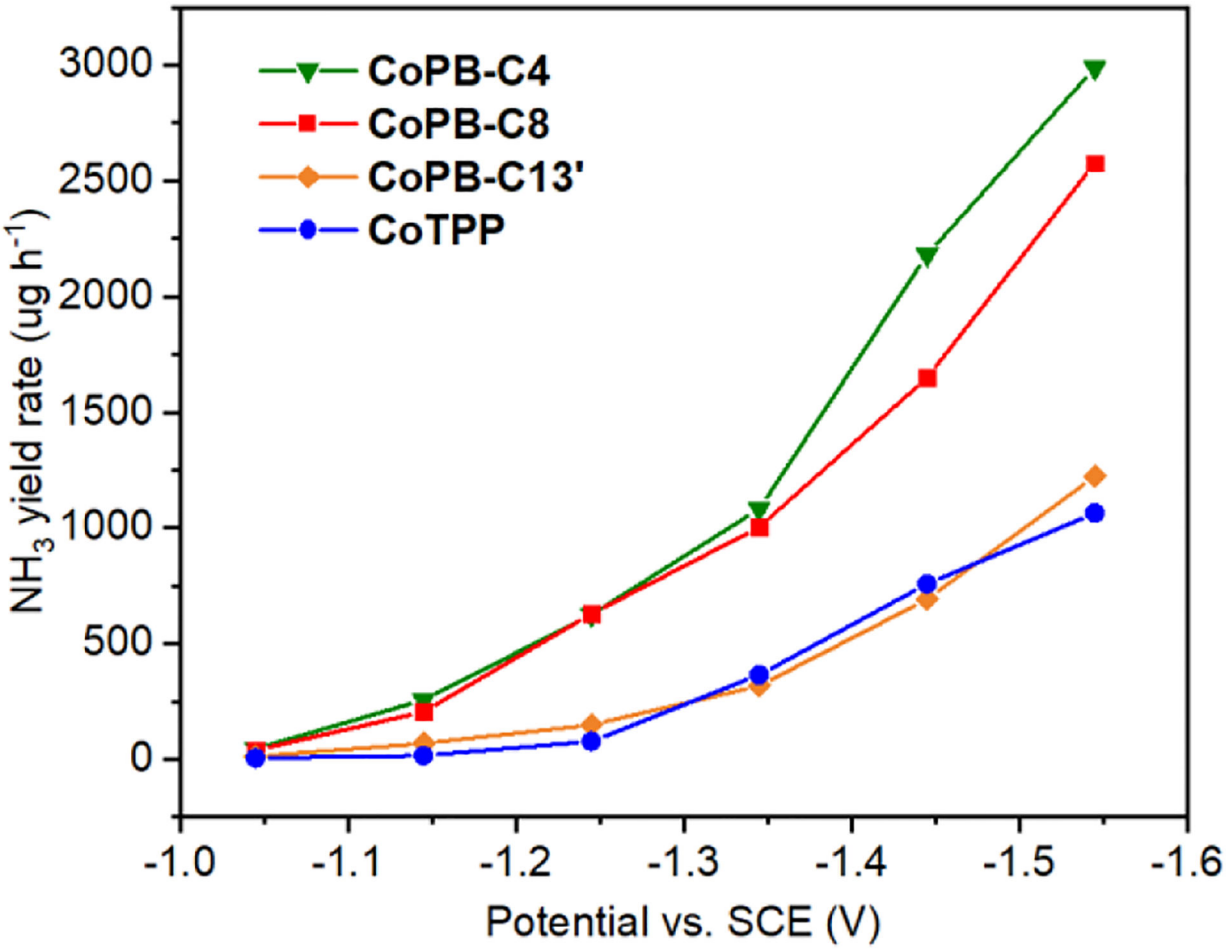

Figure 4.

The effect of peripheral alkyl substituents on the eNO_3RR activity of CoPBs. NH_3 yield rate comparison for **CoPB-C4** (green), **CoPB-C6** (purple), **CoPB-C8** (red), **CoPB-C13'** (orange), and **CoTPP** (blue).

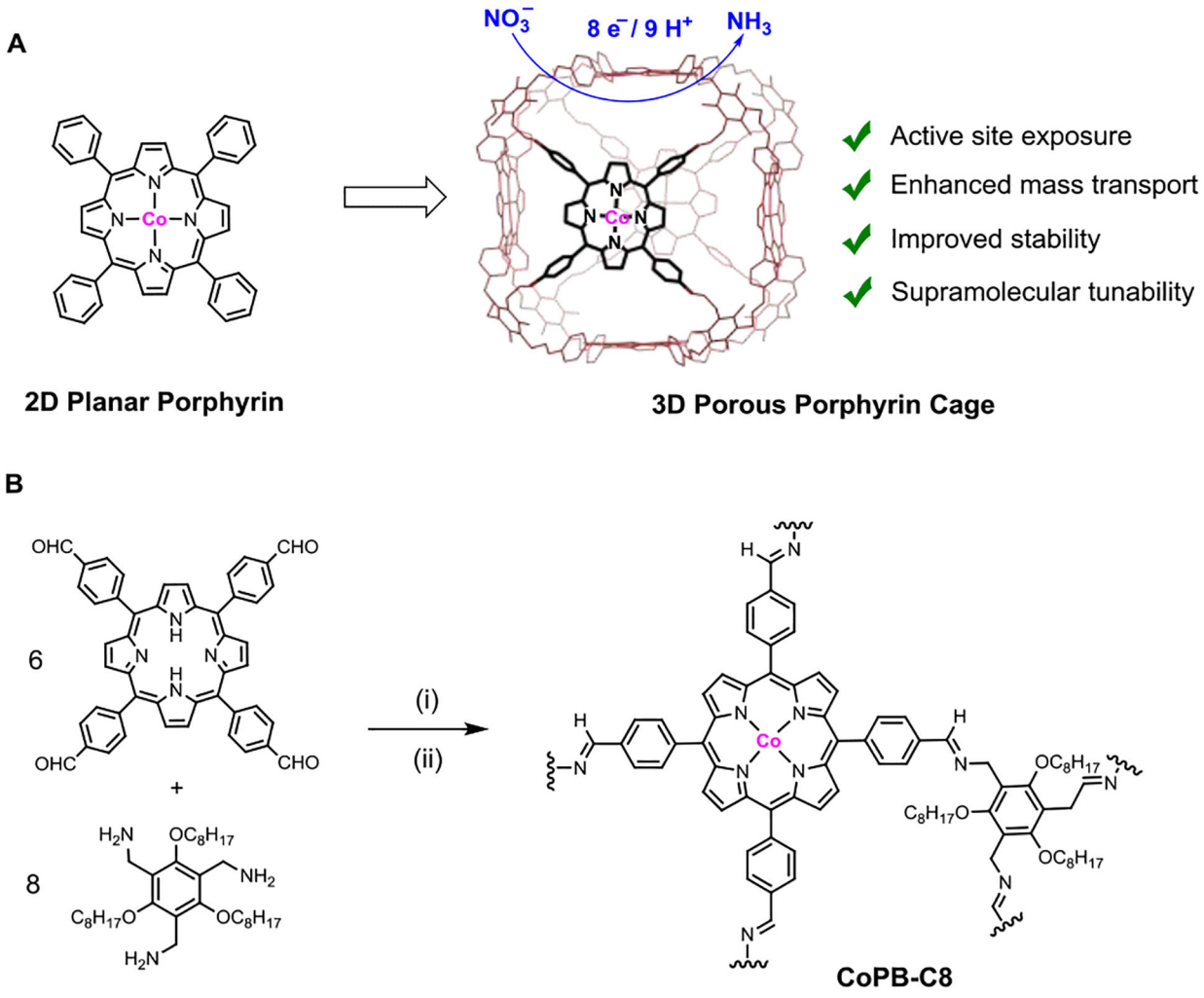

Scheme 1.

(A) Supramolecular enhancement of electrochemical NO_3RR catalyzed by embedding 2D molecular cobalt porphyrin into a 3D porous organic cage architecture. (B) Synthesis of the CoPB-C8. (i) trifluoroacetic acid (TFA), $CHCl_3$, 60 °C, 24 h, 90%; (ii) $CoCl_2$, 2,6-lutidine, THF, 70 °C, 48 h, 95%.